crystals

MDPI

Article

High-Performance Piezoelectric Characteristics of Sm Substituted $Pb(Ni,Nb)O_3$-$Pb(Zr,Ti)O_3$-$Pb(Mg,W)O_3$ System Ceramics for Ultrasonic Transducer Application

Sujin Kang [1], Jonghyeon Lee [1], Juhyun Yoo [1,*], Sun A. Whang [2], Suho Lee [3], Seonghoon Kee [4,*], Inho Im [5] and Changwoo Oh [6]

[1] Department of Electrical Engineering, Semyung University, Jechon 27136, Korea; sujin95k@nate.com (S.K.); ljh2391@nate.com (J.L.)
[2] Department of Nursing, Semyung University, Jechon 27136, Korea; sawhang@semyung.ac.kr
[3] Department of Electrical Engineering, Dong-A University, Busan 49236, Korea; shlee@dau.ac.kr
[4] Department of ICT Integrated Ocean Smart Cities Engineering, Dong-A University, Busan 49236, Korea
[5] Department of Electrical Engineering, Shinansan University, Ansan 15435, Korea; iminho@sau.ac.kr
[6] Substrate Manufacture, Amosense, Cheonan 31040, Korea; ocw3040@amosense.co.kr
* Correspondence: juhyun57@semyung.ac.kr (J.Y.); shkee@dau.ac.kr (S.K.)

Abstract: In this paper, in order to develop composition ceramics for an acoustic emission sensor application for nondestructive testing, $Pb(Ni,Nb_{2/3})O_3$-$Pb(Zr,Ti)O_3$-$Pb(Mg,W)O_3$ [PNN-PZT-PMW] system ceramics were manufactured by conventional mixed oxide method using Li_2CO_3 and $CaCO_3$ as sintering aids. Their microstructural, dielectric and piezoelectric properties were also investigated. At x = 0.0075 Sm, the substituted specimen sintered at 980 (°C), and high values of piezoelectric properties appeared: the dielectric constant (ε_r) of 2824, piezoelectric coefficient d_{33} of 630 [pC/N], planar electromechanical coupling factor k_p of 0.665, piezoelectric voltage constant g_{33} of 25.2 [mV.m/N], and high Curie temperature (Tc) = 270 (°C), respectively. These values were applicable for devices such as acoustic emission sensor and ultrasonic transducer.

Keywords: acoustic emission sensor; nondestructive testing; piezoelectric coefficient d_{33}

Citation: Kang, S.; Lee, J.; Yoo, J.; Whang, S.A.; Lee, S.; Kee, S.; Im, I.; Oh, C. High-Performance Piezoelectric Characteristics of Sm Substituted $Pb(Ni,Nb)O_3$-$Pb(Zr,Ti)O_3$-$Pb(Mg,W)O_3$ System Ceramics for Ultrasonic Transducer Application. *Crystals* **2022**, *12*, 738. https://doi.org/10.3390/cryst12050738

Academic Editor: Weili Deng

Received: 29 April 2022
Accepted: 17 May 2022
Published: 20 May 2022

1. Introduction

An acoustic emission is defined as an elastic wave that is emitted due to changes in the sudden elastic field in the material mediums. The source of acoustic emission can become the production and movement of the magnetic domain and the creation and growth of a micro-crack. That is, when the energy accumulated by the change of the elastic field is suddenly emitted, acoustic emission can be possible. These acoustic emission techniques can be not only used as a means of measuring the information of the materials in which it is difficult to be measured in the microscopic phenomena for a material test or a characteristic evaluation, but also as a non-destructive test such as a crack detection. From the perspective of non-destructive examination for structure health monitoring, other non-destructive test methods such as ultrasonic testing can observe the reaction result of the materials by injecting ultrasonic energy from an outside power source, while acoustic emission techniques can be evaluated by measuring the self-emitting signal using an acoustic emission sensor [1]. Additionally, the nondestructive testing method using an ultrasonic transducer is a very useful method because it can observe the structural defect of the test materials without damaging the testing subject [2]. In particular, ultrasonic energy is very effective in enhancing micro-circulation and improving the metabolism by increasing the tissue temperature through the generation of its thermal energy. Ultrasonic energy can be delivered to the subcutaneous fat cells to break down the fats cells, and this means that the amount of subcutaneous fats will be reduced through the excretion

of people. Accordingly, an ultrasonic transducer can be used as the piezoelectric device mounted with ultrasonic physical therapy machine [3].

Piezoelectric PZT system ceramics have been widely used as, for example, piezoelectric sensors, piezoelectric resonators, ultrasonic transducers for ultrasonic physical therapy machines, and piezoelectric haptic actuators. In particular, acoustic emission sensors, ultrasonic transducers for nondestructive testing, and ultrasonic physical therapy machines require higher kp and higher d_{33} for further increasing an electro mechanical conversion efficiency and generating displacement. We reported the excellent values of kp = 0.648, d_{33} = 379 [pC/N], g_{33} = 38.2 [mV. m/N]) in $Pb(Ni_{1/3}Nb_{2/3})O_3$-$Pb(Zr,Ti)O_3$ system ceramics [2]. Here, we selected the $Pb(Ni_{1/3}Nb_{2/3})O_3$-$Pb(Zr,Ti)O_3$ system ceramics widely used for piezoelectric devices due to its high piezoelectric d_{33} constant. Recently, in order to increase the piezoelectric performance of $Pb(Zr,Ti)O_3$ and Pb-free (Na,K) NbO_3 ceramics, many ternary composition system ceramics have been developed such as PNN-PZT, PMN-PZT, PZN-PZT, $(K,Na)(Nb,Sb)O_3$-$(Bi,Na)ZrO_3$-$BaZrO_3$ etc [4–16]. Moreover, instead of $Pb(Ni_{1/3}Nb_{2/3})O_3$, $Pb(Ni_{1/3}Nb_{2/3})O_3$-$Pb(Zr,Ti)O_3$ composition system ceramics can increase the piezoelectric properties for the application devices such as energy harvesters and actuators by various kinds of additional compounds such as $Pb(Mg,W)O_3$ and $Pb(Ni,W)O_3$ [1,4,7,8]. Recently, H. Jia, et al. reported a highest d_{33} = 870 pC/N in PZN-PMN-PT system [17].

For the purpose of the application of an acoustic emission sensor for nondestructive testing and ultrasonic transducer for ultrasonic physical therapy machine [3], $Pb(Ni,Nb)O_3$-$Pb(Zr,Ti)O_3$-$Pb(Mg,W)O_3$ ceramics were selected, and Sm was substituted for enhancing the piezoelectric properties of the ceramics, and then were fabricated [18], and their piezoelectric and microstructural characteristics were investigated.

2. Experimental

$Pb_{(0.985-1.5x)}Sm_x$ $(Mg_{1/2}W_{1/2})_w(Ni_{1/3}Nb_{2/3})_y(Zr_{0.50}Ti_{0.50})_zO_3$–0.015 Bi (x = from 0 to 0.0125, w = 0.03, y = 0.09, z = 0.88) + Sintering aids (Li_2CO_3 + $CaCO_3$) ceramics were synthesized by conventional solid state reaction methods.

Sm_2O_3, PbO, ZrO_2, TiO_2, NiO, WO_3, Nb_2O_5, Bi_2O_3, and MgO were selected as raw materials with additional 1.5 mol% Bi substitution of Pb site in the composition formula Mall-milling for 24 h. Additionally, then, calcination was performed for 2 h at 850 °C. Li_2CO_3 and $CaCO_3$ were added as the sintering aids.

A 5%PVA (polyvinyl alcohol) was added to the dried powders. The dried powders were molded by the pressure of 15 MPa in a mold with a diameter of 17 mm, burned out at 600 °C for 3 h. They were sintered at 930 (°C)~980 (°C) for 2 h. Using the Archimedes method, the bulk density of specimens was calculated by measuring specimen weight in air (B) and water (A),by following the formula: ρ(density) = [B/(B − A)], respectively. The specimens were polished to 1 mm thickness with about 14 mm diameter and then electrodeposited with Ag paste. The poling process was performed at 120°C in a silicon oil bath by applying the electric field E = 30 kV/cm. The grain size and crystal structure of specimens were measured by a scanning electron microscope (SEM: Model Hitachi, S-2400, Yeongwol, Korea) and X-ray diffraction (XRD: Rigaku, D/MAX-2500H), respectively. In order to measure temperature dependence of dielectric constant (ε_r), specimens were mounted in the electric furnace. Then, the capacitance was measured at 1 kHz using an LCR meter (ANDO AG-4034), and the temperature dependence of dielectric constant (ε_r) as a function of Sm substitution was calculated. Piezoelectric constant d_{33} was measured using d_{33} m (APC 8000). Then, piezoelectric voltage constant g_{33} was calculated by $g_{33} = d_{33}/(\varepsilon_r.\varepsilon_o)$. Additionally, frequency constant Np (kHz.mm) was calculated by fr .D (resonant frequency (fr) diameter). The piezoelectric properties were investigated using an Impedance Analyzer (Agilent 4294A Electromechanical coupling factor kp were calculated [19]. Then, Qm were calculated according to IRE standard [20].

3. Results and Discussion

X-ray diffraction patterns with Sm substitution are shown in Figure 1a,b. Pure perovskite phase appeared in all the specimens. A rombohedral-tetragonal (R-T) phase coexistence appeared in all the specimens. An (002) tetragonal peak and a (200) rhombohedral peak are shown in Figure 1a narrow angle range. Here, the intensity of the (002) tetragonal peak was slightly increased with increasing Sm substitution. These phenomena can be explained by the conclusion that Sm^{3+} ion did not react as donor dopant by the substitution for Pb^{2+} ion site and was segregated at the grain boundary due to the excessive Sm substitution [21].

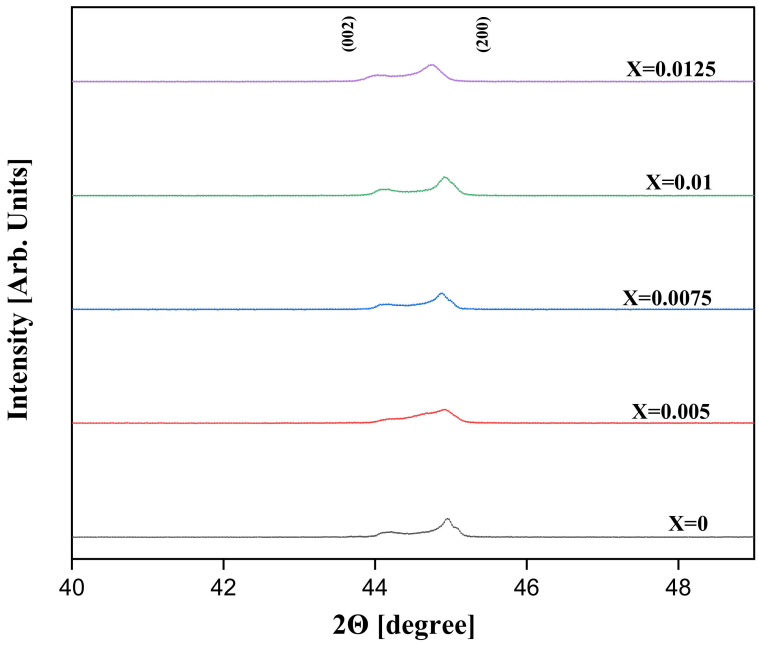

(**a**)

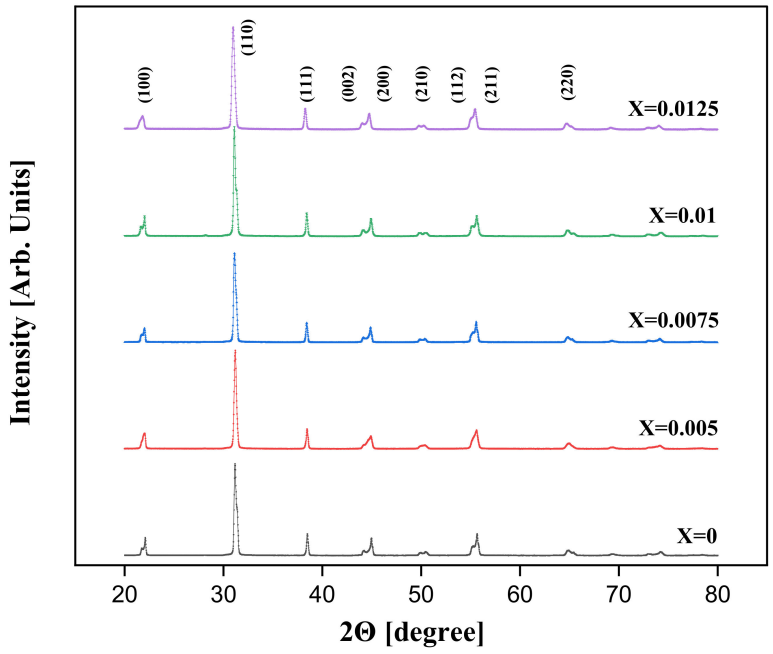

(**b**)

Figure 1. XRD pattern with Sm substitution ((**a**) narrow angle range (**b**) wide angle range).

The microstructure of specimens with the amount of Sm substitution is shown in Figure 2. The grain sizes showed the values of 6.3 μm, 3.58. μm, 5.65 μm, 2.94 μm, and 3.06 μm with increasing Sm substitution as x = 0 0.005, 0.0075, 0.01, and 0.0125, respectively. At the x = 0 Sm substitution, the highest grain size of 6.3 μm appeared. The Li_2CO_3 and $CaCO_3$ addition as the sintering aids with the eutectic point of 662 (°C) can enhance the densification of the ceramics by performing the liquid phase formation. However, with increasing Sm substitution, the optimal sintering temperature of the ceramics was increased from 930 °C to 980 °C due to the solubility limit because Sm substitution was additionally done except for 1.5 mol% Bi substitution of the ceramics, as shown in Table 1. Figure 3 shows density with Sm substitution. The highest density of specimens was increased up to 7.855 g/cm^3 at the sintering temperature of 980 °C and x = 0.0075, and thereafter decreased. These results can be illustrated by the fact that the solubility limit temperature of the ceramics was increased, owing to Sm substitution. Figure 4a,b show an impedance curve and k_p according to Sm substitution, respectively. The k_p of specimens increased according to the increasing amount of Sm substitution. The impedance curve and k_p of specimens sintered at 980 (°C) are shown. The kp increased to the highest value of 0.665 at x = 0.0075 Sm, while kp = 0.640 at x = 0 Sm and the excellent wide Δf(fa-fr) widths between resonant frequency fr and anti-resonant frequency fa at x = 0.0075, respectively, and then decreased due to the excess Sm substitution. That is, the Δf(fa-fr) widths between fr and fa showed values of 29.68 (kHz), 30.11 (kHz), 31.63 (kHz), 11.2 (kHz), and 18 (kHz) with increasing Sm substitution as x = 0, 0.005, 0.0075, 0.01, and 0.0125, respectively. The large distance between fr and fa can generate a high vibration in the case of manufacturing the ultrasonic transducer for ultrasonic physical therapy machine.

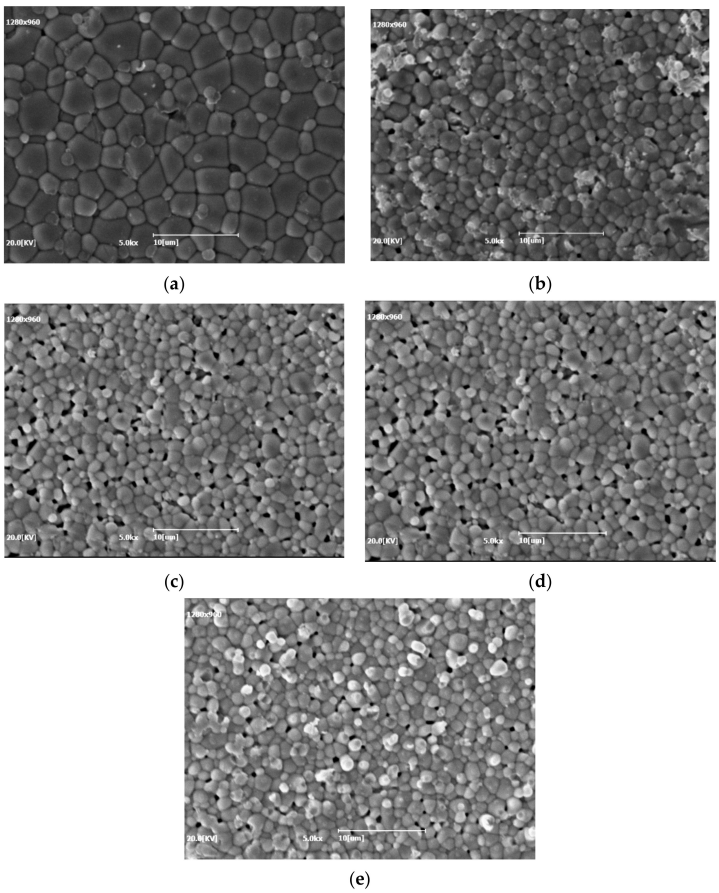

Figure 2. SEM micrographs with Sm substitution (**a**) x = 0. (**b**) x = 0.005 (**c**) x = 0.0075 (**d**) x = 0.01 (**e**) x = 0.0125.

Table 1. Physical properties with Sm substitution.

Optimal Sintering Temp. (°C)	X	Density [g/cm^3]	k_p	Dielectric Constant	d_{33} [pC/N]	g_{33} [mV.m/N]	Np (KHz.mm)	Q_m	Tc (°C)
900	0	7.811	0.640	1983	508	28.9	1971	54	290
960	0.005	7.750	0.653	2682	616	25.9	1938	54	280
980	0.0075	7.855	0.665	2824	630	25.2	1927	55	270
980	0.01	7.303	0.433	1743	370	23.9	1971	71	270
980	0.0125	7.373	0.522	2059	484	26.5	1995	64	270

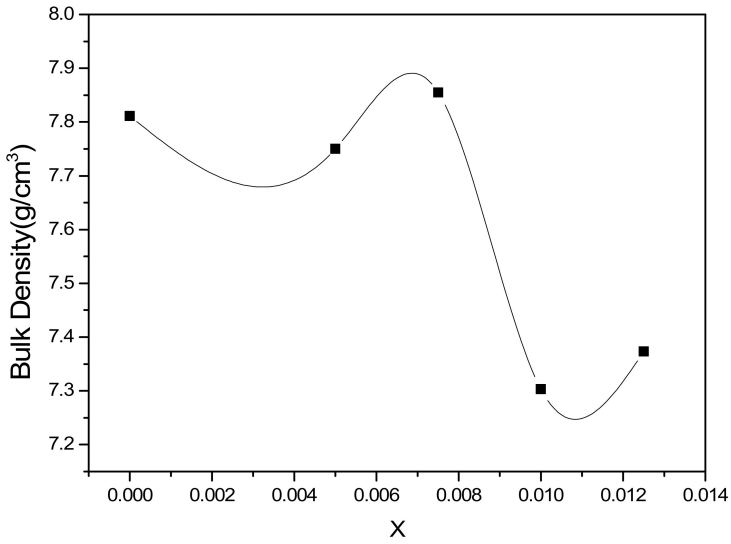

Figure 3. Bulk density with Sm substitution.

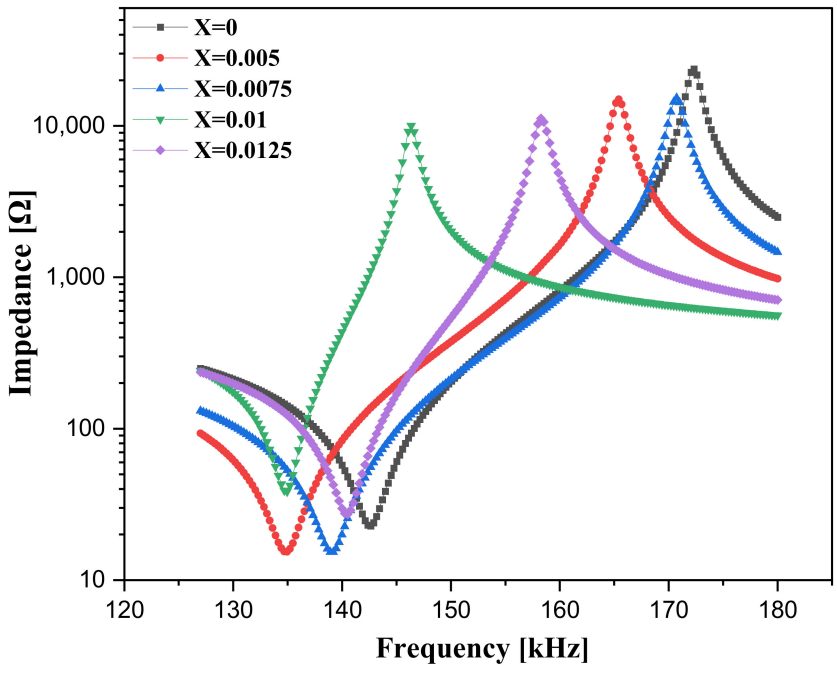

(**a**)

Figure 4. *Cont.*

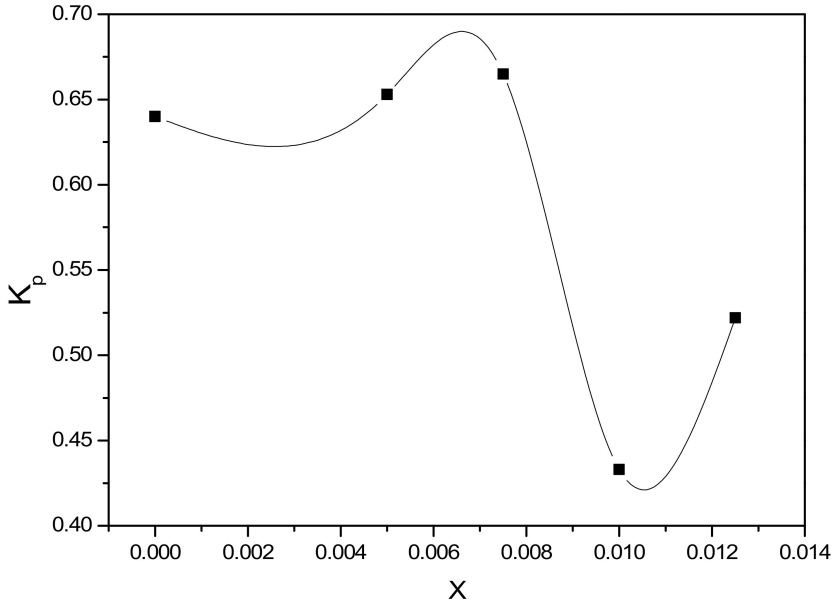

(**b**)

Figure 4. Impedance curve (**a**) and electromechanical coupling factor (k_p) (**b**) with Sm substitution.

The d_{33} and g_{33} with Sm substitution are shown in Figure 5. The d_{33} of specimens sintered at 980 (°C) enhanced up to the highest value of 630 [pC/N] at x = 0.0075 Sm, while d_{33} = 508 [pC/N] at x = 0 Sm and then decreased due to the excess Sm substitution. These phenomena can be explained by the conclusion that the Sm^{3+} ion can react as donor dopant by the substitution of Pb $^{2+}$ion sites [21]. The behavior of g_{33} showed opposite trends with d_{33} due to the differences of increasing widths of ε_r because the piezoelectric voltage constant g_{33} can be explained by $g_{33} = d_{33}/(\varepsilon_r . \varepsilon_o)$. The value of g_{33} decreased according to the amount of Sm substitution. The maximum value of g_{33} = 28.9 [mV.m/N] appeared at the x = 0 Sm substitution. Figure 6 shows the dielectric constant ε_r according to Sm substitution. The ε_r of specimens sintered at 980 (°C) also showed a maximum value of 2824 at x = 0.0075 Sm substitution and then decreased due to the excess Sm substitution. Figure 7 shows the variation of planar mode frequency constant Np (KHz.mm) according to Sm substitution. The planar mode frequency constant Np is defined as fr .D (resonant frequency (fr) .diameter). Here, the diameter of specimens showed the values of 14.09 mm, 14.40 mm, 13.87 mm, 14.66 mm, and 14.25 mm with increasing Sm substitution as x = 0, 0.005, 0.0075, 0.01, and 0.0125, respectively. The value of Np decreased up to 1927 x = 0.0075 according to the amount of Sm substitution and then again increased from x = 0.1. This minimum value of 1927 is because of high kp and high d_{33} at x = 0.0075. The highest value of Np = 1995 was appeared at the x = 0 0125 Sm substitution.

The mechanical quality factor (Q_m) with Sm substitution is shown in Figure 8. The behavior of Q_m increased according to Sm substitution. The maximum value of 71.56 appeared at the x = 0.01 Sm substitution. Here, this result is also because the Sm^{3+} ion did not react as a donor dopant, but was segregated at the grain boundary due to the excessive Sm substitution [22].

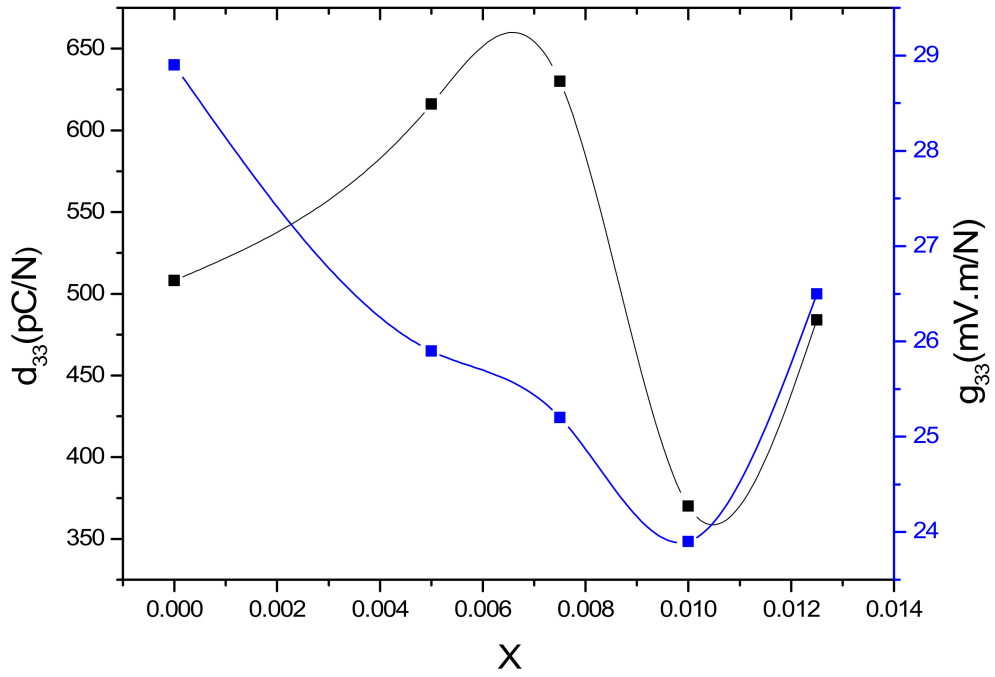

Figure 5. Piezoelectric charge constant (d_{33}) and piezoelectric voltage constant (g_{33}) with Sm substitution.

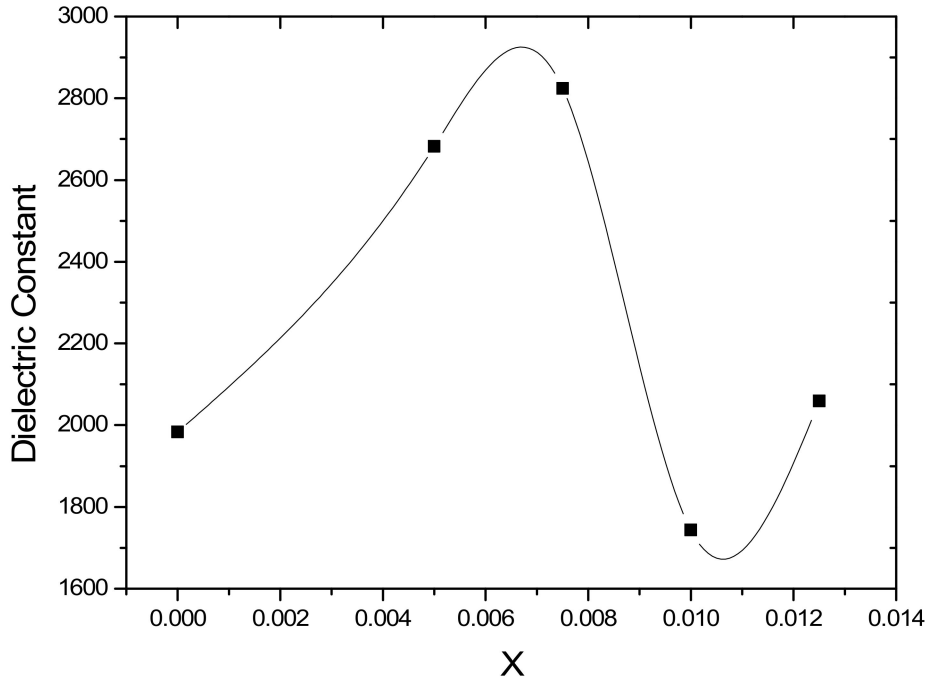

Figure 6. Dielectric constant with Sm substitution.

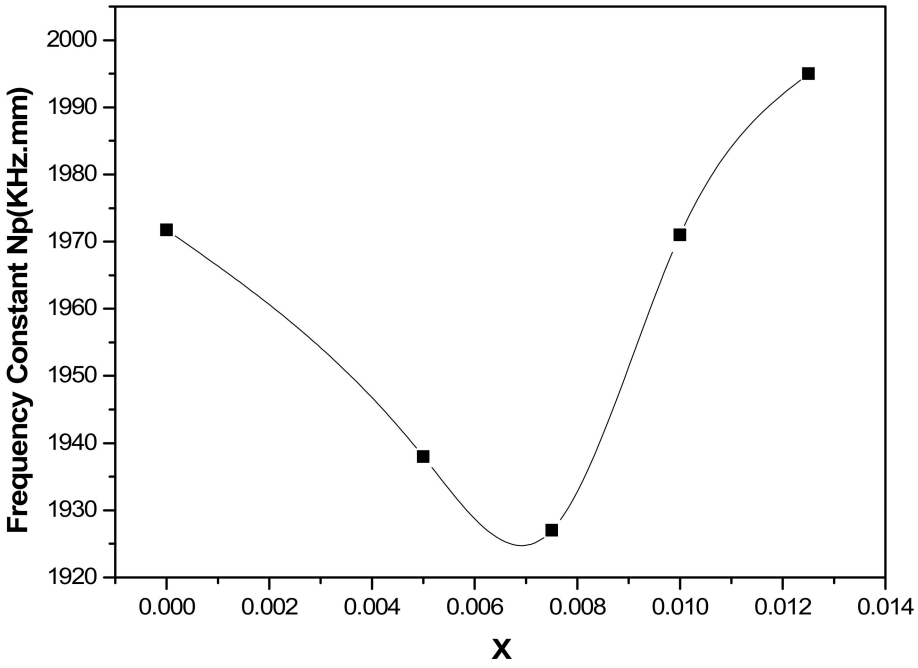

Figure 7. The variation of frequency constant Np with Sm substitution.

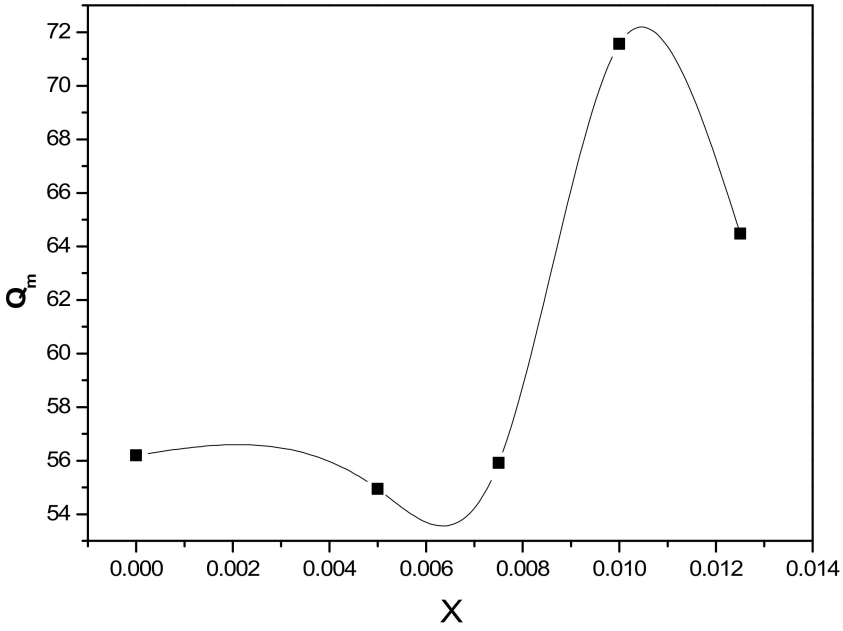

Figure 8. Mechanical quality factor (Q_m) with Sm substitution.

The temperature dependence of dielectric constant (ε_r) with Sm substitution is shown in Figure 9. The Curie temperature of the specimens slowly decreased up to x = 0.0075 according to the increase in the amount of Sm substitution. Thereafter, the Curie temperature of the specimens was constantly maintained as 270 (°C). Finally, at x = 0.0075, the Sm substituted specimen sintered at 980 (°C), and the piezoelectric properties of ε_r = 2824, d_{33} = 630 [pC/N], and k_p = 0.665 were suitable for the device application such as acoustic emission sensor and ultrasonic transducer. Table 1 shows the physical properties of specimens manufactured with the amount of Sm substitution.

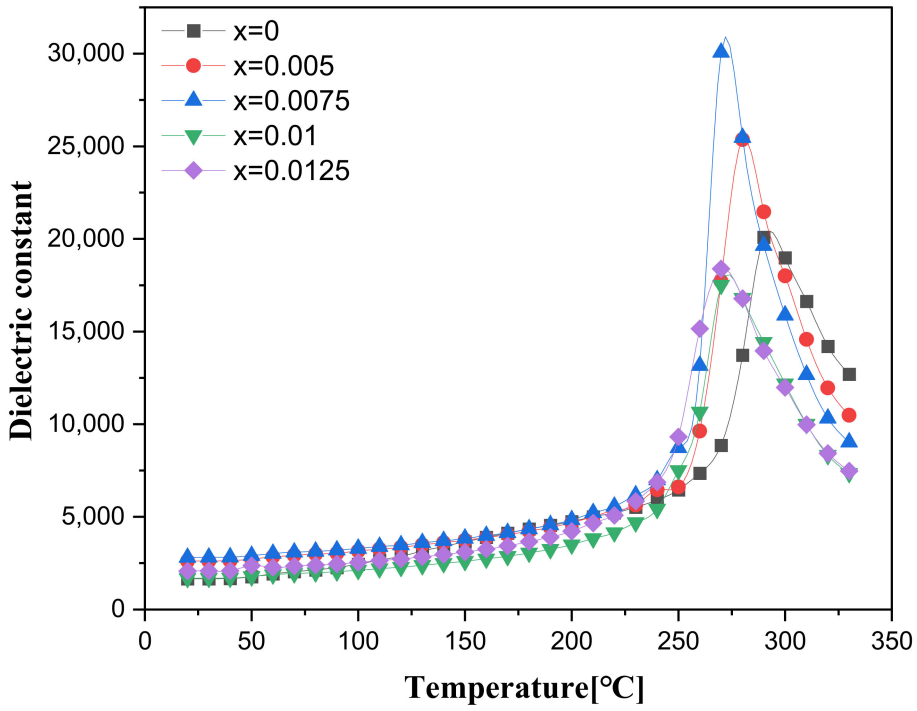

Figure 9. Temperature dependence of dielectric constant (ε_r) with Sm substitution.

4. Conclusions

For developing developed high-performance piezoelectric ceramics for the application of devices such as acoustic emission sensors and ultrasonic transducers.

$Pb(Ni,Nb)O_3$-$Pb(Zr,Ti)O_3$-$Pb(Mg,W)O_3$ ceramics were manufactured with Sm substitution. Their microstructural, dielectric and piezoelectric properties were also investigated. The experimental results are as follows:

1. Pure perovskite phase appeared in all the specimens. A rombohedral-tetragonal (R-T) phase coexistence appeared in all the specimens.
2. The surface grain sizes showed the values of 6.3 μm, 3.58. μm, 5.65 μm, 2.94 μm, and 3.06 μm with increasing Sm substitution as x = 0, 0.005, 0.0075, 0.01, and 0.0125, respectively.
3. The piezoelectric constant d_{33} of specimens sintered at 980 (°C) enhanced up to the high value of 630 [pC/N] at x = 0.0075 Sm, while d_{33} = 508 [pC/N] at x = 0 Sm.
4. At x = 0.0075, the Sm-substituted specimen sintered at 980 (°C), and high values of piezoelectric characteristics appeared: the dielectric constant (ε_r) of 2824, piezoelectric coefficient d_{33} of 630 [pC/N], planar electromechanical coupling factor k_p of 0.665, piezoelectric voltage constant g_{33} of 25.2 [mV.m/N], and high Curie temperature (Tc) = 270 (°C), respectively.

Author Contributions: Investigation, S.K. (Sujin Kang), J.L., S.A.W., S.L. and I.I.; Supervision, J.Y. funding acquisition: S.K. (Seonghoon Kee) and C.O. All authors have read and agreed to the published version of the manuscript.

Funding: This work was supported by Amosense Co., Ltd. (2022) and the Korea Agency for Infrastructure Technology Advancement (KAIA) grant funded by the Ministry of Land, Infrastructure and Transport (Grant 21CTAP-C163815-01).

Data Availability Statement: Not Applicable.

Conflicts of Interest: The authors declare no conflict of interest.

References

1. Yapar, O.; Basu, P.K.; Volgyesi, P.; Ledeczi, A. Structural health monitoring of bridges with piezoelectric AE sensors. *Eng. Fail. Anal.* **2015**, *56*, 150. [CrossRef]
2. Yoo, J.; Lee, J.; Kang, S.; Eum, M.; Lee, S.; Kee, S.H. Microstructure and Piezoelectric Properties of $Pb(Ni_{1/3}Nb_{2/3})O_3$-$Pb(Zr,Ti)O_3$ System Ceramics doped with Sb_2O_5 for Ultrasonic Nondestructive Testing Transducer. *Trans. Electr. Electron. Mater.* **2021**, *22*, 913. [CrossRef]
3. Kim, H.J.; Kim, M.H. The Effects of Kettlebell Exercise and Ultrasound Treatment on Body Mass Index and Percent Body Fat in 20′s Adults. *J. Korean Phys. Ther. Sci.* **2018**, *25*, 1. [CrossRef]
4. Yoo, J.; Lee, J. The Effects ofMnO_2 Addition on the Physical Properties of $Pb(Ni_{1/3}Nb_{2/3})O_3$-$Pb(Zr,Ti)O_3$-$Pb(Mg_{1/2}\ W_{1/2})O_3$-$BiFeO_3$ Ceramics. *Crystal* **2021**, *11*, 29. [CrossRef]
5. Lee, S.S.; Kim, K.B. Recent Research Trend for Nondestructive Testing Technology. *J. Korean Soc. Nondestruct. Test.* **2003**, *23*, 14.
6. Lee, T.-G.; Lee, H.-J.; Kim, S.-W.; Kim, D.-H.; Han, S.H.; Kang, H.-W.; Kang, C.-Y.; Nahm, S. Piezoelectric properties of $Pb(Zr,Ti)O_3$-$Pb(Ni,Nb)O_3$ ceramics and their application in energy harvesters. *J. Eur. Ceram. Soc.* **2017**, *37*, 3935. [CrossRef]
7. Sin, S.-H.; Yoo, J.-H.; Kim, Y.-J.; Baek, S.-K.; Ha, J.-S.; No, C.-H.; Song, H.-S.; Shin, D.-C. Physical properties of inorganic PMW-PNN-PZT ceramics. *IOP Conf. Ser. Mater. Sci. Eng.* **2015**, *87*, 012099. [CrossRef]
8. Bomlai, P.; Muensit, N.; Milne, S.J. Structural and electrical properties of (1-x)(Na0. 465K0. 465 Li0. 07) NbO3–x CaTiO3 lead-free piezoelectric ceramics with high Curie temperature. *Procedia Eng.* **2012**, *32*, 814. [CrossRef]
9. Jeong, Y.; Yoo, K.; Yoo, J. Piezoelectric and dielectric characteristics of low-temperature-sintering Pb (Mg1/2W1/2) O3–Pb (Ni1/3Nb2/3) O3–Pb (Zr, Ti) O3 ceramics according to the amount of PNN substitution. *J. Electroceramics* **2009**, *23*, 387. [CrossRef]
10. Ha, J.Y.; Choi, J.W.; Kang, C.Y.; Choi, D.J.; Kim, H.J.; Yoon, S.J. Effects of ZnO on piezoelectric properties of 0.01PMW-0.41PNN-0.35PT-0.23PZ ceramics. *Mater. Chem. Phys.* **2005**, *90*, 396–400. [CrossRef]
11. Kwang-Hee, Y.; Kyu-Soo, K.; Byung-Soo, C. Piezoelectric and Electric Field Induced Strain Properties of PMW-PNN-PZT Ceramics with the Substitution of Ba. *J. Korean Inst. Electr. Electron. Mater. Eng.* **2001**, *14*, 20–25.
12. Lee, K.S.; Lee, I.H.; Yoo, J.H.; Ryu, S.L. Piezoelectric and Dielectric Properties of PZW-PMN-PZT Piezoelectric Ceramic according to Sintering Aid Li_2CO_3 Addition. *J. Korean Inst. Electr. Electron. Mater. Eng.* **2007**, *20*, 1034–1038.
13. Yoo, J. High Dielectric and Piezoelectric Properties of Low-Temperature Sintering PNN-PMN-PZT Ceramics for Low-Loss Piezoelectric Actuator Application. *Trans. Electr. Electron. Mater.* **2018**, *19*, 249. [CrossRef]
14. Zhou, C.; Zhang, J.; Yao, W.; Liu, D.; He, G. Remarkably strong piezoelectricity, rhombohedral-orthorhombic-tetragonal phase coexistence and domain structure of $(K,Na)(Nb,Sb)O_3$–$(Bi,Na)ZrO_3$–$BaZrO_3$ ceramics. *J. Alloys Compd.* **2020**, *820*, 153411. [CrossRef]
15. Zhang, B.; Wu, J.; Cheng, X.; Wang, X.; Xiao, D.; Zhu, J.; Wang, X.; Lou, X. Giant Piezoelectricity in Potassium–Sodium Niobate Lead-Free Ceramics. *ACS Appl. Mater. Interfaces* **2013**, *5*, 7718. [CrossRef] [PubMed]
16. Qiao, L.; Li, G.; Tao, H. Full characterization for material constants of a promising KNN-based lead-free piezoelectric ceramic. *Ceram. Int.* **2020**, *46*, 5641. [CrossRef]
17. Jia, H.; Mi, J.; Li, Z.; Wang, L. Imprved dielectric and piezoelectric properties of Sm-doped PMN-PZN-PT ternary. *Ceram. Int.* **2022**, *48*, 14761. [CrossRef]
18. Levin, E.M.; Robbins, C.R.; Mcmurdie, H.F. *Phase Diagrams for Ceramists*; The American Ceramic Society: Columbus, OH, USA, 1964; Volume 158.
19. Dong, Y.; Yue, Q.; Cheng, D.; Zhou, Z.; Liang, R.; Dong, X. Ultrasonic transducer with BiScO3-PbTiO3-based ceramics of operating temperature over 400 °C IRE standards on piezoelectric crystals: Measurement of piezoelectric ceramics. *Sens. Actuators* **2022**, *49*, 1161.
20. Berlincourt, D.; Kinsley, T.; Lambert, T.M.; Schwartz, D.; Gerber, E.A.; Fair, I.E. IRE standards on piezoelectric crystals: Measurement of piezoelectric ceramics. *Proc. IRE* **1961**, *49*, 1161–1169.
21. Fan, G.F.; Shi, M.B.; Lu, W.Z.; Wang, Y.Q.; Liang, F. Effects of Li_2CO_3 and Sm_2O_3 additives on low-temperature sintering and piezoelectric properties of PZN-PZT ceramics. *J. Eur. Ceram. Soc.* **2014**, *34*, 23. [CrossRef]
22. Peng, G.G.; Zheng, D.Y.; Hu, S.M.; Zhao, H.; Cheng, C.; Zhang, J. Effects of rare-earth Sm_2O_3 addition on relaxation behavior and electric properties of 0.5PNN-0.5PZT ceramics. *J. Mater. Sci. Mater. Electron.* **2016**, *27*, 5509. [CrossRef]